RAA 2019 Vol. **19** No. **7**, 90(12pp) doi: 10.1088/1674–4527/19/7/90

http://www.raa-journal.org *http://iopscience.iop.org/raa*

Research in Astronomy and Astrophysics

Long-term trends in solar activity. Variations of solar indices in the last 40 years

Elena Bruevich and Vasily Bruevich

Sternberg Astronomical Institute, Moscow State University, Universitetsky pr., 13, Moscow 119992, Russia; *red-field@yandex.ru, brouev@sai.msu.ru*

Received 2018 October 29; accepted 2018 December 17

Abstract We analyze long-term variations of several solar activity indices (AIs) that have been measured over the last 40 years. With this goal, we study the AIs that characterize the fluxes from different areas in the solar atmosphere. Our consideration of mutual correlations between the solar indices is based on the study of relationships between them in the period from 1950 to 1990. This period of time, covering activity cycles 19–22, is characterized by relatively stable relations between the indices. We investigate the normalized variations of these indices in recent time in relation to their values which were calculated by considering radiation from the Sun in the radio range at a wavelength of 10.7 cm ($F_{10.7}$) in 1950–1990. The analysis of time series, representing variations of the normalized AI (AIFF) in solar cycles 23–24, shows different trends exist for different indices in terms of their long-term behavior. We assume that variations of normalized International Sunspot Number (SSN), $F_{530.3}$ and Flare Index, which have shown sharp decreases in the last 40 years, are possibly associated with a decrease in the intensity of large-scale magnetic fields in the photosphere (SSN) and in the corona (the coronal index and the Flare Index).

Key words: method: data analysis — Sun: activity indices

1 INTRODUCTION

The magnetic field of the Sun is the main source of variability for solar radiation. Dominant periodic variations known as Schwabe (11-yr) and Hale (22-yr) cycles show a strong connection with the structure and evolution of the magnetic field. A link between solar magnetic field evolution and variation of the activity index (AI), which are associated with photosphere and corona, can be explained by the concept of magnetic helicity. Magnetic helicity is one of the so-called invariants of motion in magnetohydrodynamics (that is, the value of the physical quantity associated with some physical process which does not change over time). This idea has been used to explain some phenomena that are related to solar activity (Pevtsov et al. 2011).

Variations in solar AI are closely interconnected, so that variations in the magnetic field are the sources of these changes. Stars of late-type spectral classes are also characterized by a relatively close correlation between the radiation fluxes emanating from the star's photosphere, chromosphere and corona (Bruevich & Alekseev 2007).

Hathaway (2015); Pevtsov et al. (2014) report that the 24th activity cycle is much weaker than cycles 21, 22 and 23. We can see that according to observations of the International Sunspot Number (SSN) in cycles 23, 24 and possibly during the next cycle 25, the Sun is characterized by low activity, see Figure 1.

We see that the current minimum of activity is similar to the Dalton Minimum. This minimum was characterized by low solar activity which occurred during solar cycles 4–7 (from 1790 to 1830). Some scientists also suggested that soon solar activity according to SSN values in cycles 25–26 will be also very low (SSN will be about 50–70 in the cycle's maximum) like the low solar activity that happened during the Dalton or Maunder Minimums (Casey 2014). It has also been asserted that this current minimum results from the superposition of the 11-yr minimum with the minima of cycles with 50-yr and 100-yr periods. Usoskin & Mursula (2003) also suggested that a long-term decrease in solar activity is influenced by the current minimum of the 100-yr Gleissberg cycle.

The Mount Wilson Observatory has been observing Sun-like stars as part of the HK project during the past 50 years, focusing on their chromospheric activity cycles.

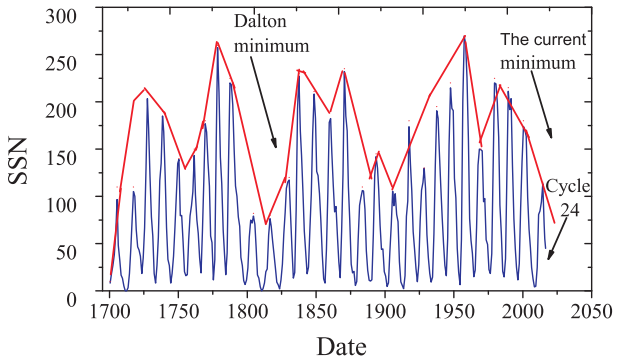

Fig. 1 SSN – yearly SSN. Observations for 1700–2017.

The analysis of stellar data sets has indicated that stars with clearly defined solar-type cycles have chromospheric fluxes which correspond to Maunder Minimum-like conditions about 25% of the time (Baliunas et al. 1995).

We are currently nine years into cycle 24. Solar cycle 24 is almost completely passed and the Sun is now approaching to its next minimum in activity. The current observed values of maximum amplitudes in solar index variations indicate that this cycle is the smallest since cycle 14 (Pesnell 2012). In cycle 24 we can see a "double-peaked" solar maximum. The second maximum was in April 2014 (smoothed values of SSN reached 116.4). This second peak of SSN surpassed the first peak (smoothed values of SSN reached 98.3 in March 2012). Cycle 24 is an unusual cycle in which the second maximum (according to SSN observations) was larger than SSN in the first maximum. For SSN, it was shown that there are opposite long-scale trends during solar cycles 22–24. Nagovitsyn et al. (2012) analyzed previous SSN observations from Penn & Livingston (2006); Pevtsov et al. (2011).

Nagovitsyn et al. (2012) also demonstrated that number of spots with large areas decreases, while the number of spots with small areas grows. This behavior can be explained by a gradual decrease in magnetic field strength in sunspots. This assumption agrees well with the observational data, see Penn & Livingston (2006).

A cycle's evolution can be studied by examining variation of the empirical function which connects the SSN and $F_{10.7}$ in cycles 23–24.

The ratio of the observed $\mathrm{SSN}^{\mathrm{obs}}$ to that predicted by $\mathrm{SSN}^{\mathrm{synt}}$, using the previously established relationship with $F_{10.7}$ flux for the period from 1950 to 1990 when the relationships between solar indices were stable, is called the sunspot formation fraction (SFF). This quantity was introduced by Livingston et al. (2012),

$$\mathrm{SFF} = \mathrm{SSN}^{\mathrm{obs}}/\mathrm{SSN}^{\mathrm{synt}} \ . \qquad (1)$$

For different solar indices, in this paper we determine the AI formation fraction (AIFF), which is similar to the SFF parameter, corresponding to a ratio of the AI observed to the AI predicted. For calculations that predict AI, we use a previously established relationship to $F_{10.7}$ flux from the Table 1 below. We determine AIFF as

$$\mathrm{AIFF} = F_{\mathrm{ind}}^{\mathrm{obs}}/F_{\mathrm{ind}}^{\mathrm{synt}} \ . \qquad (2)$$

The close relationships between the solar indices observed from 1950 to 1990 could be considered to be well established.

A significant deviation from these relationships in cycles 23 – 24 from previous relationships in 1950–1990 can be employed in the study of long-term trends in relationships between the indices (Livingston et al. 2012).

According to Livingston et al. (2012), the average magnetic field in sunspots in 1990–2008 decreased by 25%. Later, Watson et al. (2014) examined some of the properties of sunspot umbrae over the period 1997–2014 with three different instruments on the ground and in space: MDI, HMI and BABO. It was shown that annual average magnetic field in the darkest part of sunspot umbrae decreased continuously, from approximately from 2800 G in 1998 to 2100 G in 2008, and then stabilized and remained equal to 2200 G until 2014.

Since magnetic fields in sunspots have decreased, the sunspots are becoming not so cold and then their temperature contrast with the surrounding photosphere (which is usually 1500 K) is getting smaller, which makes some spots less visible. Consequently, the Total Solar Irradiance (TSI) might increase a bit, see Svalgaard (2013); Bruevich et al. (2014).

The minimum of solar activity between cycles 23 and 24 was very long because the decline phase of cycle 23 was unusually long. The solar AI, which was introduced at San Fernando Observatory, is based on photometric images obtained at this observatory. This value represents a combination of areas of sunspots and faculae. Areas of sunspots and faculae are easy to observe, and these indices describe the current state of solar activity well. In Chapman et al. (2014), it was shown that areas of sunspots in cycles 22, 23 and 24 changed as 1.0, 0.74 and 0.37 respectively.

In Figure 1 we see the yearly data on SSN for 1700–2017. Note that the 1700–1850 data are the results of indirect assessments. In Figure 1, also we can see three well-defined cycles of activity: the main cycle of activity (this cycle is approximately equal to a 10–11 yr) and the 40–50 yr cyclicity with the 100–120 yr (ancient) cyclicity (according to the solid line connecting the maxima of the 11-yr cycle).

We can also ascertain that the trend displayed in Figure 1 (using a thick solid line) indicates a progressive decrease in SSN during the last 50 years. The study of near-surface structural changes in recent cycles implies that there is some possibility of long-term variation in solar dynamo parameters (Howe et al. 2017).

Table 1 Indices of Solar Activity and Their Observation Data Archives

Activity Index	Area of Formation	Interval of Obs.	Website with Archive Data
$F_{10.7}$	Corona	1975–2017	*https://www.ngdc.noaa.gov/stp/solar/solardataservices.html*
SSN	Photosphere	1975–2017	*http://www.ngdc.noaa.gov/stp/sunspot-numbers/international/*
$F_{\mathrm{Ly}-\alpha}$	Chromosphere	1975–2017	*http://lasp.colorado.edu/lisird/tss/composite_lyman_alpha.html*
MgII c/w	Chromosphere	1975–2017	*http://www.iup.uni-bremen.de/UVSAT/Datasets/mgii*
$F_{530.3}$	Corona	1975–2008	*https://www.ngdc.noaa.gov/stp/solar/corona.html*
TSI PMOD	Photosphere	1978–2017	*https://www.pmodwrc.ch/pmod.php?topic=tsi/composite/SolarConstant*
TSI ACRIM	Photosphere	1975–2017	*ftp://ftp.ngdc.noaa.gov/STP/SOLAR_DATA/SOLAR_IRRADIANCE/ACRIM3/*
Flare Index	Corona	1975–2016	*ftp://ftp.ngdc.noaa.gov/STP/SOLARDATA/SOLARFLARES/INDEX*

In Table 1, we can view consolidated information on solar AIs and websites where observational data are available.

In Janardhan et al. (2010), the National Solar Observatory Kitt Peak synoptic magnetograms were analyzed for cycles 21–23. These indicated that the absolute values of the polar fields decreased during cycle 23 compared to cycles 21 and 22.

The aim of our paper is to examine long-term variations of AI, which are important in the study of solar-terrestrial connections in cycles 21–24. Main trends in long-term changes (on the time scale of 30–50 years) differ for the studied solar indices. This fact points to various mechanisms of formation and temporal evolution of solar indices.

Figure 2 depicts the time series of observations of solar activity indices which are analyzed in this work. For example, in Figure 2(a) we plot monthly SSN for cycles 21–24. The data were obtained from the available websites, see the related information in Table 1.

2 THE RELATIONSHIP BETWEEN SOLAR ACTIVITY INDICES AND $F_{10.7}$ IN 1950–1990

Tobiska et al. (2000) pointed out that variations of the TSI, solar ultraviolet (UV), solar extreme ultraviolet (EUV) and solar soft X-rays are the fundamental mechanisms causing variations in main parameters describing the terrestrial atmosphere, land and oceans.

First, we analyze an interconnection between activity indices SSN, MgII c/w (core to wing ratio), TSI composite (PMOD and ACRIM), H Lyman-α 121.6 nm flux and Flare Index versus $F_{10.7}$ for the 1975–1990 data.

The $F_{10.7}$ index is flux at the wavelength of 10.7 cm (2800 MHz) which comes from the full disc of the Sun. Compared with SSN, the $F_{10.7}$ index has the following advantages: it is a measure of real flux (so it is more objective) and it can be measured in any weather.

Note that in the period from 1950 to 1990, solar AI showed consistent and stable interrelations (Svalgaard 2013). In Deng et al. (2013), the analyses of phase asynchrony between 10.7 cm solar radio flux and SSNs during the period of February 1947 to June 2012 were done. Related studies investigated a phase asynchrony between coronal index and SSNs. Deng et al. (2013) found that the SSNs begin one month earlier than coronal index. This effect of asynchrony for AI versus $F_{10.7}$ (the value of asynchrony is on the order of a month) introduces a small additional variance to values in the relations linking the AIs to the 10.7 flux studied in our paper, see Figure 4(a) (SSN versus $F_{10.7}$) and Figure 7(a) (coronal index versus $F_{10.7}$). Meanwhile, the choice of $F_{10.7}$ to describe the average value of activity on the Sun seemed to us the most acceptable in order to study solar indices using normalized values, as was successfully done in Svalgaard (2013). If we take into account the effect of asynchrony between AI and 10.7 cm flux, then according to our estimates, this would slightly reduce the standard deviations in determining the regression coefficients. However, the changes in values of the regression coefficients and their errors (see Table 2) are small enough for our task. When we calculate relative normalized indices AIFF, this effect generally becomes indistinguishable.

An interconnection between activity indices (in the period from 1950 to 1990 when solar AI showed a stable interrelation (Svalgaard 2013)) corresponds to the polynomial regression equation

$$F_{\mathrm{ind}}^{\mathrm{synt}} = a_{\mathrm{ind}} + b1_{\mathrm{ind}} \cdot F_{10.7} + b2_{\mathrm{ind}} \cdot F_{10.7}^2 \,, \qquad (3)$$

where $F_{\mathrm{ind}}^{\mathrm{synt}}$ is the calculated AI flux, and a_{ind}, $b1_{\mathrm{ind}}$ and $b2_{\mathrm{ind}}$ are polynomial coefficients.

In Table 2, the coefficients of polynomial regression (a, $b1$, $b2$) for solar activity indices versus $F_{10.7}$ in 1950 – 1990 (when solar AI manifested stable interrelations) are presented . We have estimated the residual sum of squares (RSS) both for linear and polynomial regressions of the AI versus $F_{10.7}$.

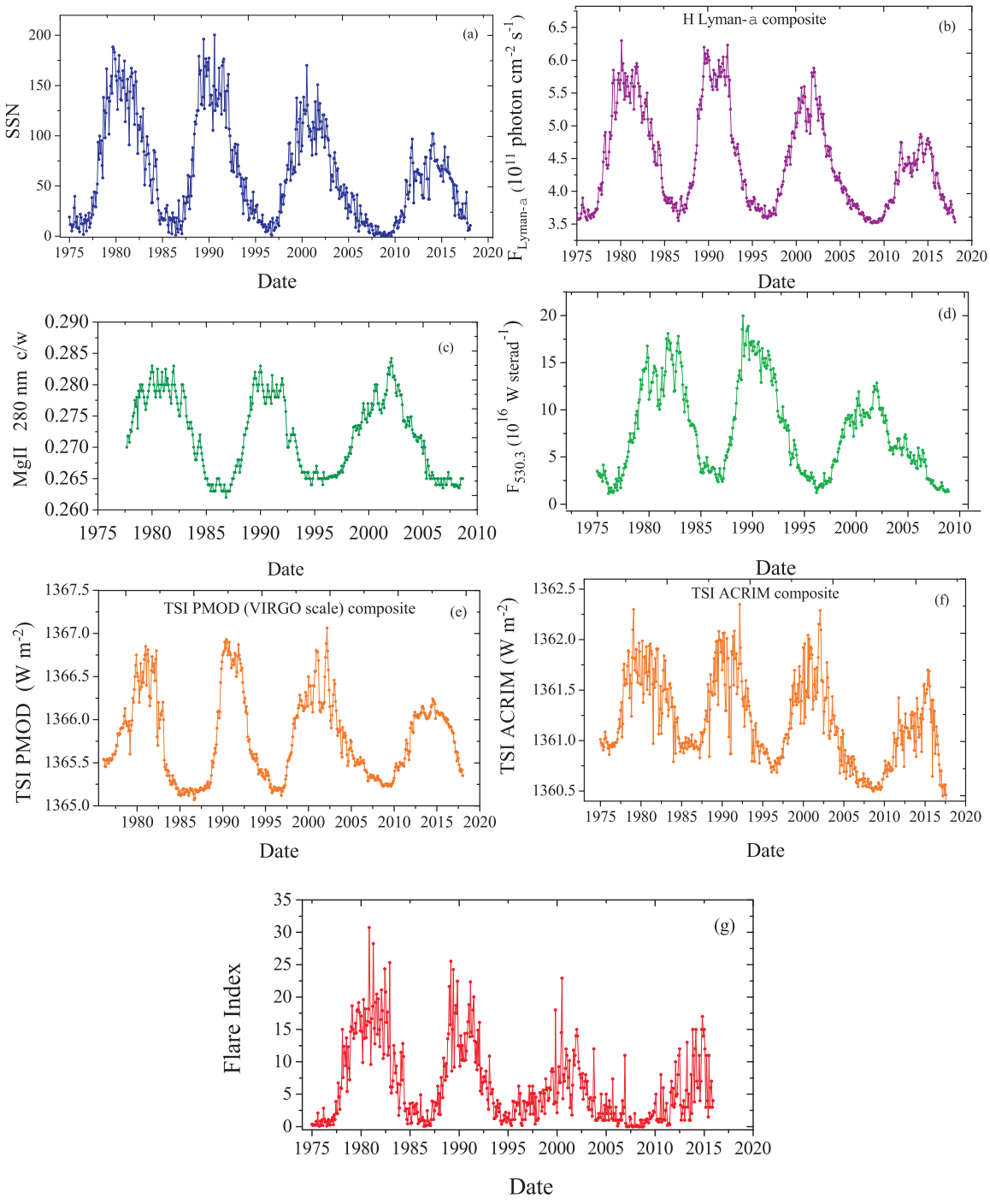

Fig. 2 (a) SSN, the 1975–2017 data; (b) H Lyman-α flux composite ($F^{\rm obs}_{{\rm Ly}-\alpha}$), the 1975–2017 data; (c) MgII 280 nm c/w Bremen composite, the 1975 – 2017 data; (d) $F_{530.3}$, the 1975–2008 data; (e) TSI PMOD composite (VIRGO scale), the 1978–2017 data; (f) TSI ACRIM composite, the 1975–2017 data; (g) Flare Index, the 1975 – 2017 data.

In this paper, we use a polynomial regression for $F^{\rm synt}_{\rm ind}$ calculations from Equation (3). Linear and polynomial regressions of AI versus $F_{10.7}$ are displayed in Figures 4(a) – 10(a) below. For different AIs, we calculated the AIFF which is equal to $F^{\rm obs}_{\rm ind}/F^{\rm synt}_{\rm ind}$ according to Equation (1), where $F^{\rm synt}_{\rm ind}$ is computed with Equation (2). Time dependencies of AIFF in the period from 1990 to the present show main trends in long-term changes of solar activity indices. It is evident that the AIFF remained close to 1 until about 1990, but the AIFF for different indices varied in different ways from 1990 to the present, see Figures 4(b) – 10(b) below.

Table 2 Coefficients of Polynomial Regression from Eq. (3) for Different AI Versus $F_{10.7}$ with 1950–1990 Observations

$F_{\rm ind}$ (AI)	a	$b1$	$b2$	σ_a	σ_{b1}	σ_{b2}
SSN	-82.56	1.39	-0.0011	3.2	0.05	0.00016
$F_{{\rm Ly}-\alpha}$	2.01	0.0264	-4.3×10^{-5}	0.166	0.0027	9.2×10^{-6}
MgII c/w	0.134	2.7×10^{-4}	-5.46×10^{-7}	0.0018	2.8×10^{-5}	9.55×10^{-8}
$F_{530.3}$	-9.7	0.203	-0.00041	1.1	0.022	7.6×10^{-5}
TSI PMOD	1364.5	0.01065	-7.13×10^{-6}	0.198	0.001	0.8×10^{-7}
TSI ACRIM	1359.9	0.0179	-4.6×10^{-5}	0.137	0.0022	7.7×10^{-6}
Flare Index	-1.358	0.0019	0.00042	0.046	0.00015	8.8×10^{-5}

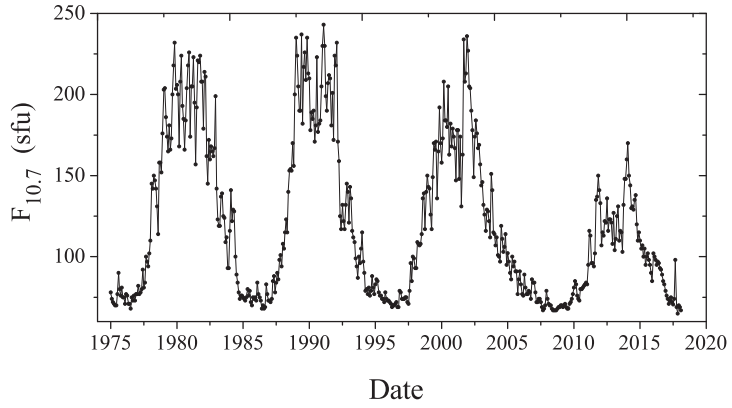

Fig. 3 The $F_{10.7}$ global index. Observations are for 1975–2017.

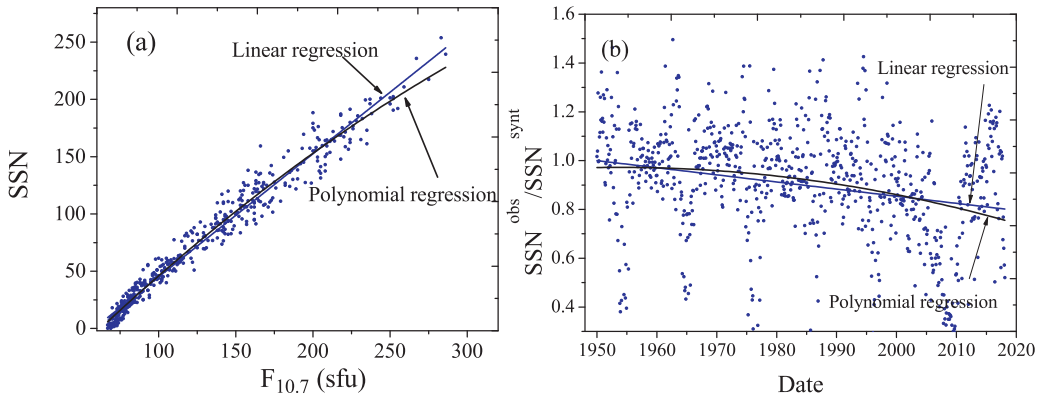

Fig. 4 (a) SSN versus $F_{10.7}$ for the period from 1950 to 1990; (b) AIFF for SSN (SFF)–$\rm SSN^{obs}/SSN^{synt}$ for the period from 1950 to 2017.

2.1 The $F_{10.7}$ Global Index

The $F_{10.7}$ index is the most suitable index for solar activity estimation and forecasting. The $F_{10.7}$ index along with SSN has one of the longest running records of solar activity. This very popular global index is measured currently in Penticton, British Columbia.

$F_{10.7}$ is a useful indicator of the solar atmosphere's emissions which are created by radiant solar active regions and whose energies are very important for the formation of Earth's thermosphere. The close correlation of EUV – $F_{10.7}$ is often used in many related atmospheric models (Tobiska et al. 2008).

It has been shown that the 10.7 cm emission can be separated into the following components: temporal events that are caused by flares with about an hour duration, and long-term variations with durations up to years and the constant component of the minimum value – Quiet Sun Level (Tobiska et al. 2008). Donnelly et al. (1983) pointed out a good correlation of $F_{10.7}$ with full-disc flux in CaII and MgII lines. EUV solar emissions act on Earth's ionosphere and modify it. These emissions correlate well with the $F_{10.7}$. UV emissions which influence Earth's stratosphere are also correlated with the $F_{10.7}$ index (Chapman & Neupert 1974; Bruevich & Nusinov 1984; Lean 1987).

Unlike many solar indices, the $F_{10.7}$ radio flux can easily be measured reliably on a day-to-day basis from

Earth's surface, in all types of weather. Reported in "solar flux units" (sfu), $F_{10.7}$ can vary from 67–68 sfu, to above 300 sfu depending on the phase of a solar cycle.

We used NASA data on $F_{10.7}$ index from the National Geophysical Data Center (NGDC) website, see Table 1. In Figure 3 we can see the $F_{10.7}$ monthly data for cycles 21–24. It is evident that for the $F_{10.7}$ index, as in the case of SSN in Figure 1, the maximum of the amplitude in cycle 24 is approximatively two times less than that in cycles 21–23.

2.2 SSN

Sunspots are transient events on the Sun's photosphere. We can view sunspots as dark areas compared to the surrounding surface.

Sunspots are places with strong concentrations of local magnetic fields. These powerful magnetic fields inhibit convection, so spots on the solar surface are regions with lowered temperature. The series of direct SSN observations has continued for more than two hundred years.

In 1850, R. Wolf defined the relative SSN as $R = 10 \times$ Number of Groups + Number of Spots which an observer can see on the solar disk.

Svalgaard & Cliver (2010) recognized that most solar AI values are closely correlated with SSN. In our paper, we use SSN data from the NASA NGDC website, see Table 1.

In Figure 4(a) we display monthly SSN versus $F_{10.7}$ for the period of stable interconnections between solar indices (1950 – 1990). The linear regression correlation coefficient for SSN versus $F_{10.7}$ is high (equal to 0.96). Using the time dependence of the SFF–$\mathrm{SSN^{obs}/SSN^{synt}}$, we examine long-term trends in normalized variations of the SSN-index.

We have also estimated RSS both for the linear and polynomial regressions of the SSN versus $F_{10.7}$ (Fig. 4(b)). The RSS has a lower value for the polynomial regression. So, a polynomial regression best describes the temporal variation in $\mathrm{SSN^{obs}/SSN^{synt}}$.

According to the trend that is displayed by the linear regression, the normalized SSN-index ($\mathrm{SSN^{obs}/SSN^{synt}}$ in Fig. 4(b)) steadily decreases from 1950 to the present time, approximately from 1 to 0.8.

We assume that the tendency which is displayed by the polynomial regression represents more than a short-term trend. The polynomial trend demonstrates that the normalized SSN-index $\mathrm{SSN^{obs}/SSN^{synt}}$ has stayed almost constant from 1950 to 1990 and has been equal to 1. However, in the period from 1990 to 2017, the $\mathrm{SSN^{obs}/SSN^{synt}}$ changed dramatically, from 1 to 0.7, which agrees with the SSN study in Nagovitsyn et al. (2012). Thus, polynomial fit of normalized SSN data indicates that there has been a sharp decrease in the normalized SSN-index of sunspot $\mathrm{SSN^{obs}/SSN^{synt}}$ in recent times (mainly in cycles 23 and 24).

2.3 Ultraviolet Solar Emission

Solar radiation in the UV range, which varies over several temporal scales (11-yr, 22-yr, 25-d, etc.), remarkably modulates the evolution of Earth's ionosphere and thermosphere. The solar activity dependence of the ionosphere is a key and fundamental issue in ionospheric physics, providing information essential to understanding the variations in the ionosphere and its processes. Solar UV-flux variations are important in research on Earth's climatic impact from solar variability. Increased hard solar emissions – EUV and X-rays – are the main source of perturbations in Earth's upper atmosphere. The chromospheric density and temperature in the Sun determine the intensities of the CaII and MgII spectral lines, and the coronal density and temperature that produce the EUV and soft X-rays.

The UV-flux affects the troposphere by the photodissociation process of major constituents in the stratosphere, heating the stratosphere, which may influence tropospheric as well as stratospheric dynamical processes (Donnelly et al. 1983).

The F2 peak in Earth's ionosphere, which is characterized by the maximum value of electron density, has a close correlation with solar activity in EUV (Liu et al. 2011). Solar short-wave flux also affects the critical frequency of the F2 layer (foF2), the plasma temperature, thermosphere winds and other important parameters used for climatic forecasts parameters of Earth's upper atmosphere. The best relationship is exhibited by fluxes in the EUV and MgII 280 nm c/w index.

The variability in solar EUV-UV radiation during the solar cycle affects the state of Earth's upper atmosphere more noticeably than the more powerful radiation in the optical range that passes through the ionosphere, practically without affecting it.

EUV-UV emission lines dominate significantly over emission in the continuum part of the solar spectrum. These emissions are formed under conditions of non-local thermodynamic equilibrium. They are formed in the high temperature layers of the solar atmosphere (transition region and low corona).

The shorter the range of emission is, the higher the amplitude of long-term variability. The change during a solar cycle reaches factors of 2 for irradiance in the 10–120 nm range, then reaches 1%–10% for 120–400 nm irradiance and the change in solar cycle is less than 1% for the TSI (Lean 1987; Tobiska et al. 2000).

Emission at 121.6 nm (H Lyman-α) mainly affects the mesosphere of the Earth. H Lyman-α photons photoionize NO molecules and form the D-region of the ionosphere. H Lyman-α emission also actively participates in the process of water vapor dissipation, after which active hydroxyl radicals are produced.

The effect of HeII 30.4 nm photons on heating of Earth's thermosphere is the most important. The flux in the HeII 30.4 nm line correlates most closely with the fluxes in lines of the UV part of the solar spectrum (Bruevich & Nusinov 1984). In this regard, study of the flux in the Lyman-alpha line $F_{\mathrm{Ly}-\alpha}$ and its cyclic variations is a very important task for forecasting the state of Earth's thermosphere.

In our paper, we use the data set of the Composite Solar Lyman-alpha which was compiled at the University of Colorado. These data are available at the website, see Table 1.

These data are based on observations from satellites TIMED and SOURCE, combined with earlier missions SME, AE-E and NOAA. All the data were calibrated to the Upper Atmosphere Research Satellite (UARS) SOLSTICE level.

In Figure 2(b) we see composite observed H Lyman-α flux data – ($F^{\mathrm{obs}}_{\mathrm{Ly}-\alpha}$). It is apparent that the absolute values of $F^{\mathrm{obs}}_{\mathrm{Ly}-\alpha}$ in cycle 24 are about 30% less than those in cycles 21–23.

In Figure 5(a) we show monthly $F^{\mathrm{obs}}_{\mathrm{Ly}-\alpha}$ versus $F_{10.7}$ for the period of stable relations between solar indices during 1950–1990. The linear regression correlation coefficient is high (equal to 0.94). It is also very high as in the case of dependencies, as displayed in Figure 4(a).

The time dependence of AIFF for H Lyman-α irradiance, $F^{\mathrm{obs}}_{\mathrm{Ly}-\alpha}/F^{\mathrm{synt}}_{\mathrm{Ly}-\alpha}$ (LalFF) in Figure 5(b), exhibits a long-term trend in normalized variation of the $F_{\mathrm{Ly}-\alpha}$-index. According to the trends that are displayed both by linear and polynomial regressions, we see that the normalized $F_{\mathrm{Ly}-\alpha}$-index (LalFF) remains constant (with an accuracy of 2%–3%) and has been about 1 in recent times.

The MgII c/w index is relatively odd among indexes. This index includes information about both the solar chromosphere (the cores of MgII lines are located at 279.56 and 280.27 nm) and about the solar photosphere (wings of MgII lines).

Solar MgII c/w is used for evaluating the common level of solar activity (Floyd et al. 2005). The MgII c/w index also has a close correlation with other UV-EUV indices (Viereck et al. 2001).

NOAA was established in 1978 and ENVISAT was launched on 2002. The NOAA and ENVISAT MgII c/w observation data are in a good agreement with Skupin et al. (2005). We used the long-term series data set from NOAA, GOME, SCIAMACHY and GOME-2 which have been combined into a single composite time series, available from the University of Bremen, see Table 1.

For convenience, this composite will be referred to as the Bremen composite. In addition to scaling the datasets, there have been a number of additional corrections to the observations in this composite (Snow et al. 2014).

In Figure 2(c), we show MgII c/w Bremen composite data. It is apparent that in cycles 21–23, the maximum amplitudes of MgII c/w exceeded the average value by about 15%, but in cycle 24 the maximum amplitude of MgII c/w exceeded the average by about 8%–10%.

In Figure 6(a), we show monthly MgII c/w versus $F_{10.7}$ for the period 1950–1990. The correlation coefficient of the linear regression is also very high, equal to 0.92.

The time dependence of normalized MgII c/w index (MgIIFF) – MgII c/w$^{\mathrm{obs}}$/MgII c/w$^{\mathrm{synt}}$ in Figure 6(b) manifests trends which are displayed by both linear and polynomial regressions. We see that the normalized MgII c/w-index remains approximately constant and recently has been about 1. In comparison with the normalized $F_{\mathrm{Ly}-\alpha}$-index, which shows a very weak downward trend, the normalized MgII c/w-index displays a very weak increasing trend.

2.4 Coronal Flux at a Wavelength of 530.3 nm

Solar flux at 530.3 nm ($F_{530.3}$) emitted by a green corona (FeXIV, 530.3 nm) is a commonly used index for solar activity that was introduced as the so-called coronal index by Rybansky (1975). Variations of this index are associated with evolution of bright structures in the corona which are characterized by different times of existence. Datasets of 530.3 nm flux are available for 1975–2008 at NGDC's website, see Table 1.

In Deng et al. (2015), the interconnection of coronal index with sunspot-dependent solar AI was studied, and it was claimed that the $F_{530.3}$ can depend on variations of both the SSN and solar flares, so that $F_{530.3}$ can be more useful in investigating solar-terrestrial connections.

Variations in $F_{530.3}$ depend on the phase of the solar cycle. These variations are closely connected with solar magnetic flux variations. In Figure 2(d) we see datasets of monthly $F_{530.3}$.

It is apparent that in cycles 21–22, maximum amplitudes of the $F_{530.3}$ were approximately equal in both cycles, but in cycle 23 the maximum amplitude of $F_{530.3}$ was about 40%–50% less.

In Figure 7(a), we show monthly $F_{530.3}$ versus $F_{10.7}$ for the period 1950–1990. The correlation coefficient of the linear regression in this case is high enough and is equal to 0.90.

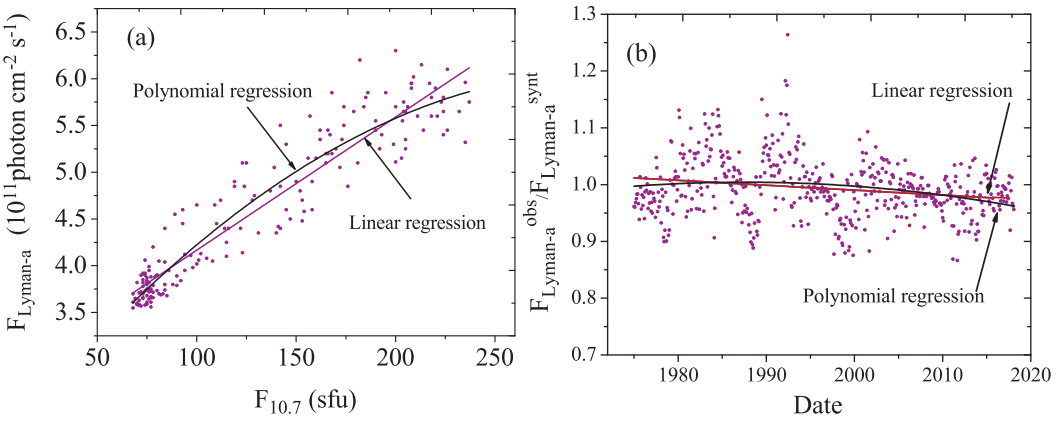

Fig. 5 (a) $F^{\rm obs}_{{\rm Ly}-\alpha}$ versus $F_{10.7}$ for the period from 1970 to 1990; (b) AIFF for H Lyman-α irradiance (LalFF) – $F^{\rm obs}_{{\rm Ly}-\alpha}/F^{\rm synt}_{{\rm Ly}-\alpha}$ for the period from 1970 to 2017.

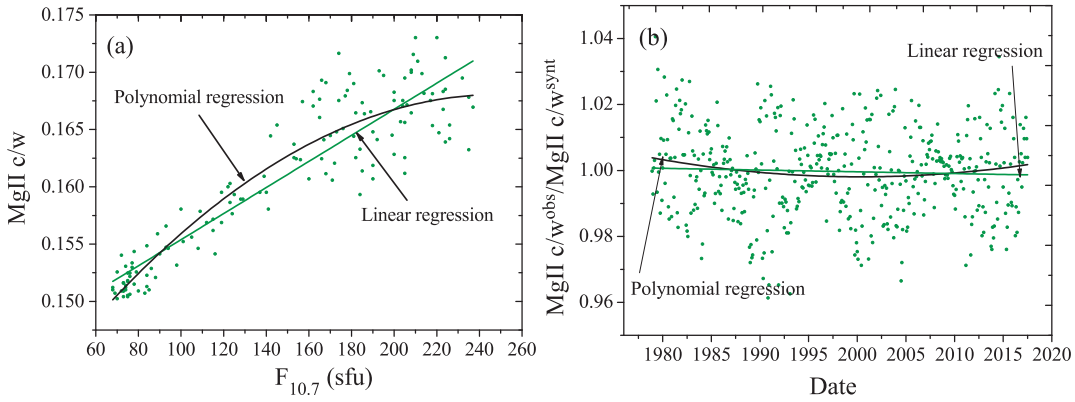

Fig. 6 (a) MgII c/w$^{\rm obs}$ versus $F_{10.7}$ for the period from 1978 to 1990; (b) AIFF for MgII 280 nm c/w irradiance (MgIIFF) – MgII c/w$^{\rm obs}$/MgII c/w$^{\rm synt}$ for the period from 1978 to 2017.

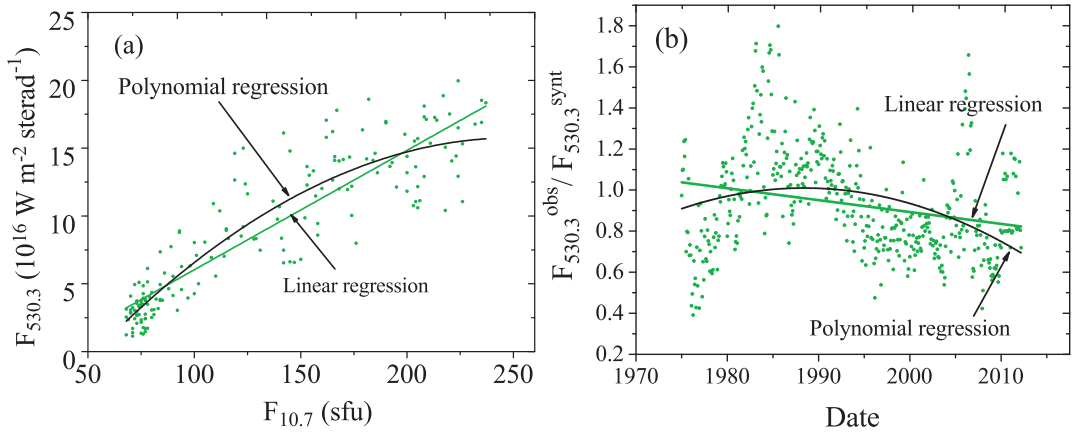

Fig. 7 (a)$F^{\rm obs}_{530.3}$ versus $F_{10.7}$ for the period from 1950 to 1990; (b) AIFF for 530.3 nm irradiance (530FF) – $F^{\rm obs}_{530.3}/F^{\rm synt}_{530.3}$ for the period from 1975 to 2008.

A time dependence of normalized $F_{530.3}$ (530FF) in Figure 7(b) manifests a long-term negative trend in relative variations of the coronal 530.3 nm flux. According to the trends which are displayed both by linear and polynomial regressions, we see that the 530FF exhibits a significant decrease by about 20% in cycle 23 as compared with the two previous cycles. In comparison with other solar activity indices (which have approximately stable AIFF values), normalized $F_{530.3}$ index 530FF displays a remarkable decrease in values.

2.5 Total Solar Irradiance

TSI, known as the Solar Constant, is the most important index related to solar activity. It is the total flux of energy of the Sun's radiation incoming to the upper part of Earth's atmosphere. Regular observations of the TSI by satellites have been carried out since 1978.

A study of reliable datasets for TSI is very important for understanding issues related to Earth's climate. It is very useful to know what contribution to warming of the climate is made by TSI in comparison with industrial gases which are expelled into the atmosphere. Krivova et al. (2003) showed that approximately 63% of changes in TSI are generated in the UV-EUV range. On average, TSI varies only about 0.1% in an 11-yr cycle. ACRIM, PMOD and other science teams have developed physics-based models of TSI variations that depend on solar activity (Krivova & Solanki 2008; Kopp et al. 2016). Two opposing processes make a contribution in TSI variability. These processes are a darkening due to sunspots and a brightening due to faculae. We will see below how long-term trends in the TSI coincide with long-term trends in fluxes of UV/EUV and in other solar AIs.

Measurements of TSI made with different equipment on different satellites have systematic errors related to special features of different measuring instruments and to their calibrations. TSI measurements were carried out on the Nimbus-7 space satellite (1978–1993) in the framework of the SMM mission on the satellite ACRIM-I (1980–1989), on the ERBS satellite (1984–1995), on NOAA satellites (1985–1989), and on the ACRIM-II and the ACRIM-III satellites (1991–2003).

Recently, instruments on space satellites from the ACRIM series in addition to VIRGO and SOHO successfully continued observations of TSI. Observations with these instruments track variations in TSI with an amplitude of about 0.2% when sunspots travel through a solar disk, while long-term variations in the solar cycle are only 0.1%. SORCE TSI data sets achieved an improved accuracy of $\pm 0.035\%$ (Dudok de Wit et al. 2017).

Inter-comparisons of different data have led to some conclusions. Willson (1997) combined the SMM/ACRIM-I data with the later UARS/ACRIM-II data by using inter-comparisons with Nimbus-7 and ERBS, and concluded that the Sun was brighter by about 0.037% during the minimum of cycle 22 than it was during cycle's 21 minimum (so-called "the trend between minima").

We used two composite data sets:

(1) PMOD composite uses Nimbus-7 and ACRIM 1–3 data on the original VIRGO scale. Datasets are available on the website, see Table 1.

(2) ACRIM composite also uses Nimbus-7/ERB, ACRIM 1–3. Datasets are available on the website, see Table 1.

A monthly plot of PMOD composite data is presented in Figure 2(e).

In Figure 8(a) we can see that a relationship between the TSI and $F_{10.7}$ is not so close as between other solar AIs and the $F_{10.7}$: a correlation coefficient for monthly TSI versus the $F_{10.7}$ is equal to 0.76 while the correlation coefficients for other AI versus the $F_{10.7}$ (in the same period 1950–1990) are equal to 0.90–0.96.

Figure 8(b) depicts the TSI PMOD$^{\rm obs}$/TSI PMOD$^{\rm synt}$ (TSIPMFF) long-term trend. We can ascertain that TSIPMFF remained relatively constant with a very weak positive trend (like for normalized $F_{\rm Ly-\alpha}$) compared to previous cycles 22–23. This trend differs from the normalized SSN and normalized $F_{530.3}$ trends, in which the AIFF significantly decreased. The trend which is elucidated in Figure 8(b) by a linear regression manifests a slight increase in the level of TSIPMFF (TSI PMOD$^{\rm obs}$/TSI PMOD$^{\rm synt}$), opposite to the SSF (SSN$^{\rm obs}$/SSN$^{\rm synt}$) trend when values reduce from 1 to 0.6. Svalgaard (2013) suggested that the recent marked reduction in the total area of spots has led to an increase of TSI. This small effect can be seen in Figure 8(b).

In Figure 2(f), we present data of ACRIM composite based on Nimbus-7, ACRIM-1, ACRIM-2, VIRGO and ACRIM-3 observations. We use the TSI data set in cycle 24, obtained from these satellites, which were compiled in NGDC and calibrated to the SORCE/TIM level.

In Figure 9(a), we see that the relationship between TSI and $F_{10.7}$ is not very close and the correlation coefficient of linear regression is equal to 0.73. Figure 9(b) demonstrates that the normalized index TSIACRFF – TSI ACRIM$^{\rm obs}$/TSI ACRIM$^{\rm synt}$ became the normalized constant with a very weak negative trend (as AIFF for $F_{\rm Ly-\alpha}$), unlike the normalized SSN and normalized $F_{530.3}$, for which the ratio AIFF became significantly lower in cycle 24. We have examined data from the TSI in two main versions and can state that the long-term trends in both cases are slightly different.

2.6 Flare Index

The Flare Index (FI) is a measure of short-lived activity on the Sun, which is approximately proportional to the total energy emitted by a flare: $FI = i \times t$, where i is the intensity scale of importance and t is the duration of the flare in minutes. Flare activity (according to monthly variations in FI) was very high in cycles 21 and 22. In cycle 23, the flare activity was two times lower. Also in the 24th cycle, the flare activity was half as much as in 23rd cy-

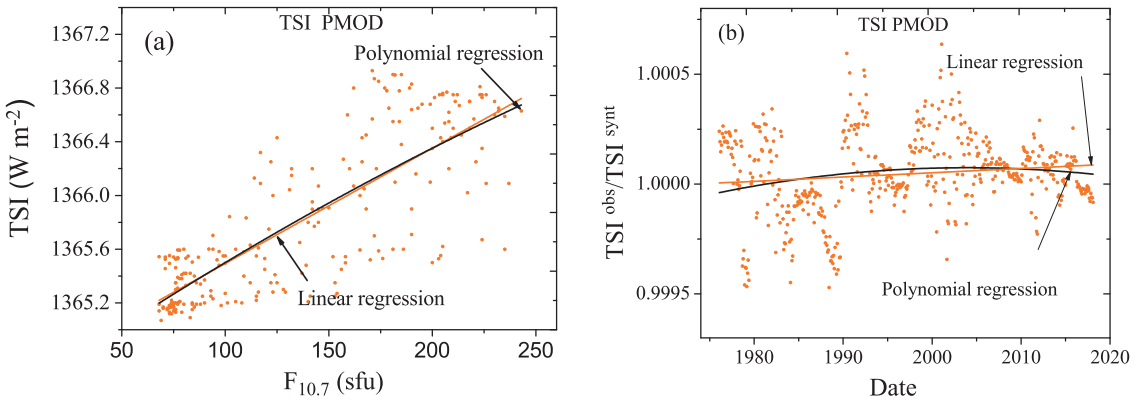

Fig. 8 (a) TSI PMOD$^{\rm obs}$ versus $F_{10.7}$ for the period from 1978 to 1990; (b) AIFF of TSI PMOD composite irradiance (TSIPMFF) – TSI PMOD$^{\rm obs}$/TSI PMOD$^{\rm synt}$ for the period from 1978 to 2017.

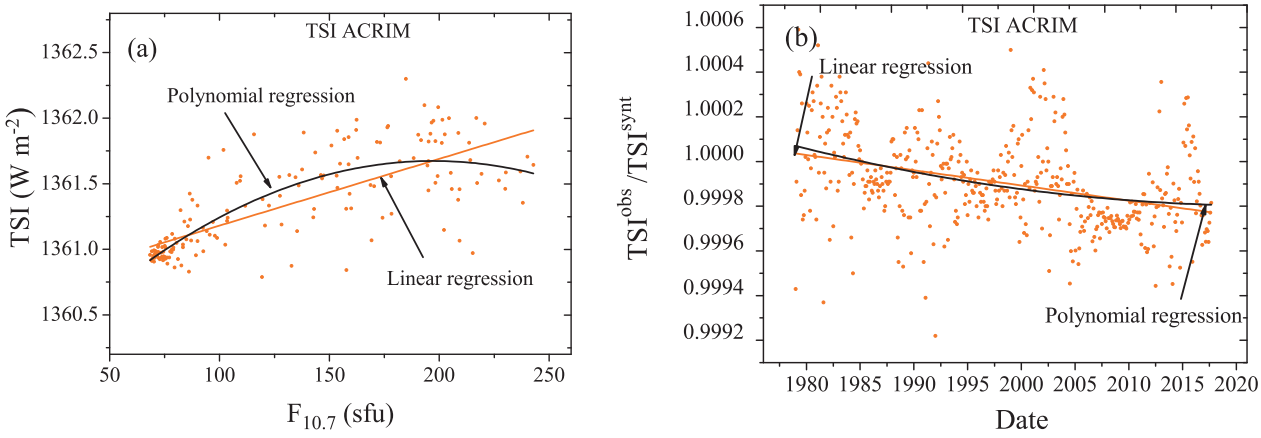

Fig. 9 (a) TSI ACRIM$^{\rm obs}$ versus $F_{10.7}$ for the period from 1975 to 1990; (b) AIFF for the TSI ACRIM irradiance (TSIACRFF) – TSI ACRIM$^{\rm obs}$/TSI ACRIM$^{\rm synt}$ for the period from 1975 to 2017.

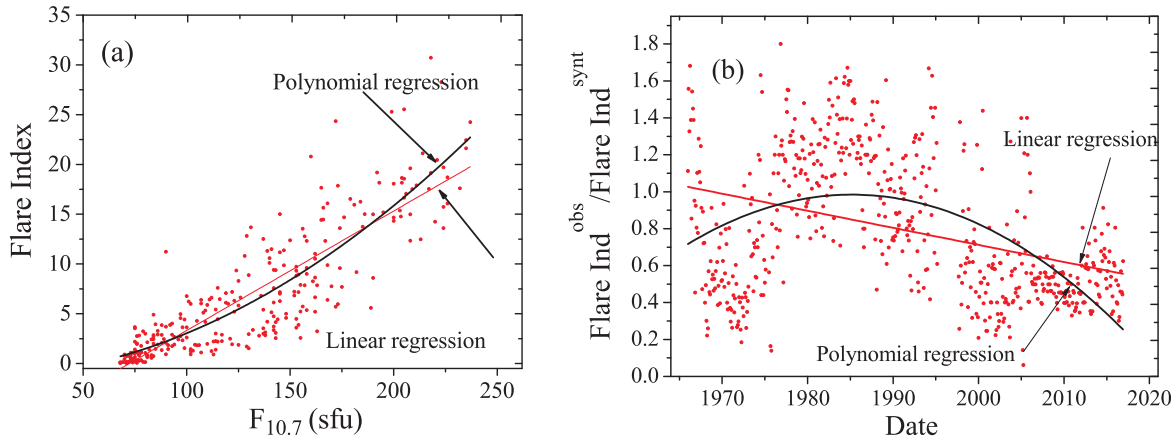

Fig. 10 (a) $FI^{\rm obs}$ versus $F_{10.7}$ for the period from 1965 to 1990; (b) AIFF for the FI (FIFF) – $FI^{\rm obs}/FI^{\rm synt}$ for the period from 1965 to 2017.

cle. A study and forecasts of the FI are necessary to evaluate the phenomenon of flare activity, since large flares lead to solar proton events, the largest of which are associated with strong magnetic storms in the Earth's magnetosphere, which can disrupt radio communications and threaten the health of astronauts.

To study the FI, we used the NASA datasets which are available on their website, see Table 1.

Atac & Ozguc (1998) compared the FI in cycle 22 with similar solar activity indices (SSN, F_{530}, $F_{10.7}$ and TSI that arise under different physical conditions) for investigating how the FI agrees with other solar indices. It was pointed out that the FI is a good indicator of solar activity on short (minutes to hours) time scales. Daily and monthly FI correlates well with daily and monthly SSN, $F_{10.7}$ and F_{530}. However, a connection between the FI and TSI is not good enough.

In Figure 2(g), we display NASA data for the FI until 2014. Note than for the period 2015 to 2017, we have calculated the FI using information from the NASA catalog on flares which has information on both flares in the optical range and flares in the X-ray range. This catalog of flare events is available at a website, see `http://www.wdcb.ru/stp/data/Solar_Flare_Events/Fl_XXIV.pdf`.

In Figure 10(a), we show monthly FI versus $F_{10.7}$ during the period of stability, 1950–1990. A correlation coefficient for the linear regression is equal to 0.87. It is high enough in comparison with the TSI versus the $F_{10.7}$ correlation.

A time dependence of the normalized FI (FIFF) in Figure 10(b) shows considerable long-term trends in FIFF. According to the linear trend, we see that the FIFF has reduced from 1 in 1970–1990 to 0.5 in 2017, but a polynomial trend exhibits a more significant reduction from 0.9–1.1 in 1970–1990 to 0.35 in 2017.

3 DISCUSSION

Our analysis shows that the determination and our further investigation of normalized AI, AIFF, have been very useful for the study and subsequent conclusions about the behavior of various AIs over activity cycles 21–24.

Note that the normalized AIFF indices should be compared with the ideal case when these values are close to 1. The noticeable differences of AIFF from 1 indicate that there are constantly changing trends for AI values that manifest as long-term trends (which the linear regression identifies) and as short-term trends (which the polynomial regression reveals) that take place.

Our study of long-term variations in the SSN-index indicates that the current 24th cycle may be a precursor of a minimum in solar activity, similar to the Dalton Minimum. This minimum of solar activity was observed in the late eighteenth – early nineteenth centuries during three consecutive cycles, see Figure 1. Thus, if cycles 25 and 26 are the same as cycle 24 or are less, the current minimum in solar activity may be similar to the Dalton Minimum. For example, Gopalswamy et al. (2018) predicted that cycle 25 will not be too different from cycle 24 in terms of its strength. This prediction for cycle 25 is based on a long-term solar activity study using microwave imaging observations from the Nobeyama Radioheliograph at 17 GHz.

We can see that variations in AI which exhibit the most decreases in normalized indices, like AIFF, are connected to the temporary variations of large-scale magnetic fields in the photosphere (the SSN) and in the corona (the $F_{530.3}$ and FI). So, the greatest changes were linked to those activity indices that are most closely related to local magnetic fields. The SSN directly depends on the number of outputs of strong magnetic fields into the atmosphere of the Sun from the convective zone under the photosphere. So, if the activity of the local magnetic field is reduced, this leads to decreasing the index of the SSN (normalized index – SSFF). The coronal index $F_{530.3}$ (normalized index – 530FF) is also closely connected to the magnetic fields because all the material in the corona is concentrated along the magnetic field lines. The growth in intensity of the magnetic field lines leads to an increase in the density and concentration of the coronal substance, which further leads to an increase in the 530.3 nm coronal flux and vice versa. The FI (normalized index – FIFF) is also closely related to magnetic fields because the flash most frequently comes from active areas (characterized by spots in the photosphere) in which the magnetic flux with the opposite sign emerges. As a result of the entanglement in the magnetic configuration of the spot, the probability of reconnection for magnetic lines at the tops of magnetic loops increases, which leads to flare release of energy.

It is also important that we have chosen to use a flux magnitude of 10.7 cm in our evaluation of the Sun's total level of radiation. The values of $F_{10.7}$ are available on the website (see Table 1) almost in real time. Measurements of this index are made with high accuracy and are constantly calibrated, which are necessary to carry out of a comparative analysis.

The $F_{10.7}$ index changes significantly (by 4–5 times) during one cycle of activity (unlike, for example, the TSI which changes by 0.1%–0.15%), and this is convenient for calculations and improves the interpretation of the analysis done.

4 CONCLUSIONS

Our analysis of different solar AIs shows the existence of short-term and long-term trends in AI time dependences over the last 40 years.

(1) Recent trends (1990–2017) demonstrate that for normalized values of the SSN, FI and $F_{530.3}$, sharp decreases exist in their normalized values SSFF, FIFF and 530FF respectively. We see that, together with reductions in their absolute values, when examining their normalized variations AIFF (which are defined

as $F_{\rm ind}^{\rm obs}/F_{\rm ind}^{\rm synt}$) additional reductions exist in the SSN, FI and $F_{530.3}$. These additional reductions have to be taken into account and should be analyzed by summarizing the expected reductions that are connected with cyclic (11-yr, half-century and century) variations in solar activity.

(2) The largest values of additional (compared to 1) decreases of normalized indices AIFF over the last 40 years show that the next AI: (1) SSN (SSFF), is approximately decreased to 20%, (2) the additional decrease in $F_{530.3}$ (530FF) is approximately equal to 30%, and (3) the FI (FIFF) has experienced an additional decrease approximately equal to 50%–70%, which is the same as for linear and for polynomial regression models.

(3) Recent trends for TSI and UV-indices (MgII c/w and the $F_{\rm Ly-\alpha}^{\rm obs}$) demonstrate that their normalized values ($F_{\rm ind}^{\rm obs}/F_{\rm ind}^{\rm synt}$ – AIFF) show an approximately constant behavior during the period 1990–2017.

(4) For the TSI PMOD composite, we see a slight increase of TSIPMFF simultaneously with a noticeable decrease of SSFF. This confirms an expectation of Svalgaard (2013) who reported the TSI should be a little larger as the dark spots on the solar disc become smaller.

Acknowledgements Our acknowledgements go to the science team of the Institute of Environmental Physics, University of Bremen for MgII c/w composite data; to the ACRIM and PMOD science teams for their corresponding TSI composites; to the Ottawa/Penticton team; to the LASP Composite Lyman Alpha science team; and to the science team of Slovak Academy of Sciences for the green corona intensity.

References

Atac, T., & Ozguc, A. 1998, Sol. Phys., 180, 397
Baliunas, S. L., Donahue, R. A., Soon, W. H., et al. 1995, ApJ, 438, 269
Bruevich, E. A., & Nusinov, A. A. 1984, Geomagnetism and Aeronomy, 24, 581
Bruevich, E. A., & Alekseev, I. Y. 2007, Astrophysics, 50, 187
Bruevich, E. A., Bruevich, V. V., & Yakunina, G. V. 2014, Journal of Astrophysics and Astronomy, 35, 1
Casey, J. L. 2014, Dark Winter: How the Sun Is Causing a 30-year Cold Spell (Humanix Books)
Chapman, R. D., & Neupert, W. M. 1974, J. Geophys. Res., 79, 4138
Chapman, G. A., de Toma, G., & Cookson, A. M. 2014, Sol. Phys., 289, 3961
Deng, L. H., Li, B., Zheng, Y. F., et al. 2013, New Astron., 23, 1
Deng, L. H., Li, B., Xiang, Y. Y., & Dun, G. T. 2015, Journal of Atmospheric and Solar-Terrestrial Physics, 122, 18
Donnelly, R. F., Heath, D. F., Lean, J. L., & Rottman, G. J. 1983, J. Geophys. Res., 88, 9883
Dudok de Wit, T., Kopp, G., Fröhlich, C., & Schöll, M. 2017, Geophys. Res. Lett., 44, 1196
Floyd, L., Newmark, J., Cook, J., et al. 2005, Journal of Atmospheric and Solar-Terrestrial Physics, 67, 3
Gopalswamy, N., Mäkelä, P., Yashiro, S., & Akiyama, S. 2018, Journal of Atmospheric and Solar-Terrestrial Physics, 176, 26
Hathaway, D. H. 2015, Living Reviews in Solar Physics, 12, 4
Howe, R., Davies, G. R., Chaplin, W. J., et al. 2017, MNRAS, 470, 1935
Janardhan, P., Bisoi, S. K., & Gosain, S. 2010, Sol. Phys., 267, 267
Kopp, G., Krivova, N., Wu, C. J., & Lean, J. 2016, Sol. Phys., 291, 2951
Krivova, N. A., Solanki, S. K., Fligge, M., & Unruh, Y. C. 2003, A&A, 399, L1
Krivova, N. A., & Solanki, S. K. 2008, Journal of Astrophysics and Astronomy, 29, 151
Lean, J. 1987, J. Geophys. Res., 92, 839
Liu, L., Wan, W., Chen, Y., & Le, H. 2011, Chinese Science Bulletin, 56, 1202
Livingston, W., Penn, M. J., & Svalgaard, L. 2012, ApJ, 757, L8
Nagovitsyn, Y. A., Pevtsov, A. A., & Livingston, W. C. 2012, ApJ, 758, L20
Penn, M. J., & Livingston, W. 2006, ApJ, 649, L45
Pesnell, W. D. 2012, Sol. Phys., 281, 507
Pevtsov, A. A., Nagovitsyn, Y. A., Tlatov, A. G., & Rybak, A. L. 2011, ApJ, 742, L36
Pevtsov, A. A., Bertello, L., Tlatov, A. G., et al. 2014, Sol. Phys., 289, 593
Rybansky, M. 1975, Bulletin of the Astronomical Institutes of Czechoslovakia, 26, 367
Skupin, J., Weber, M., Noël, S., Bovensmann, H., & Burrows, J. P. 2005, Mem. Soc. Astron. Italiana, 76, 1038
Svalgaard, L. 2013, Journal of Space Weather and Space Climate, 3, A24
Svalgaard, L., & Cliver, E. W. 2010, Journal of Geophysical Research (Space Physics), 115, A09111
Tobiska, W. K., Woods, T., Eparvier, F., et al. 2000, Journal of Atmospheric and Solar-Terrestrial Physics, 62, 1233
Tobiska, W. K., Bouwer, S. D., & Bowman, B. R. 2008, Journal of Atmospheric and Solar-Terrestrial Physics, 70, 803
Usoskin, I. G., & Mursula, K. 2003, Sol. Phys., 218, 319
Viereck, R., Puga, L., McMullin, D., et al. 2001, Geophys. Res. Lett., 28, 1343
Watson, F. T., Penn, M. J., & Livingston, W. 2014, ApJ, 787, 22
Willson, R. C. 1997, Science, 277, 1963